

Multichannel analysis of surface waves and high-resolution electrical resistivity tomography in detection of subsurface features in northwest Himalaya

A. K. Mahajan^{1,*}, Subash Chandra², V. S. Sarma² and B. R. Arora³

¹School of Earth and Environmental Sciences, Central University of Himachal, Dharamshala 176 207, India

²CSIR-National Geophysical Research Institute, Uppal Road, Hyderabad 500 007, India

³Ministry of Earth Sciences, Government of India, New Delhi 110 003, India

Geophysical studies using multichannel analysis of surface waves (MASW) and high-resolution electrical resistivity tomography (HERT) have been jointly carried out on an experimental basis in the field. The motive is to study shallow subsurface features (i.e. faults traces, cavities and palaeo-channels) in the foothill zone of Northwest Himalaya. These techniques have shown their potentiality in successfully identifying shallow (0–24 m) fault traces and dissolution features/palaeo-channels. Depending on the sensitivity of the MASW and HERT techniques, geophysical signatures of the subsurface features were recorded and further resolved with the help of synthetic simulation. The synthetic simulation of 2D electrical response has been carried out over the initial model for subsurface fault traces as well as palaeo-channels. The initial model has been refined iteratively to bring the synthetic response close to the field response and hence the final refined model is considered to be the true representation of the subsurface.

Keywords: Fault traces, high-resolution electrical resistivity tomography, multichannel analysis of surface waves, synthetic simulation, palaeo-seismology.

THE continued convergence between India and Asia is primarily absorbed by thrust motions along the three major south verging thrust faults striking along the length of the Himalayan arc (Figure 1 a). These mega thrusts from north to south are the Main Central Thrust (MCT), the Main Boundary Thrust (MBT) and the Himalayan Frontal Thrust (HFT), which separate respectively, the Higher Himalayan Crystalline meta-sediments of the Lesser Himalaya, sedimentary sequences of the Sub-Himalaya and the largely undeformed alluvial deposits in the Indo-Gangetic Plains¹. These steep dipping thrusts merge with a gentle north-dipping detachment plane, defined as the interface between the downward-moving Indian plate and the overriding sedimentary wedge of the Himalaya². This

detachment forms the seat of large and great earthquakes³. The deformation of these mega thrusts and detachments due to on-going collision of the Indian plate against the Eurasian plate, is reflected well by the occurrence of small, moderate and major earthquakes^{4,5}. Absence of primary surface ruptures during the historical earthquakes in the frontal part of the Himalayan arc, led several researchers to suggest that they are blind thrusts. Nevertheless, more recently, many trenches were excavated to search direct evidences of prehistoric fault ruptures along the 250 km long section of the HFT which have revealed vertical displacement across the scarp at a number of locations^{6–8}. The estimate of the displacement and lateral extent coupled with carbon/luminescence dating provides a measure of magnitude and date of occurrence of seismic events^{6–8}. The Himalayan frontal part is marked by high rate of sedimentation and erosion. However, the restricted depth of trench excavation limits the detection of earthquake-related deformation dating back to the past few centuries only. Further, it is likely that topography of geodynamically disturbed terrains or sub-basins is strongly modulated by the tectonics and/or climate-driven sedimentation or erosion. It is well established that tectonic and climatic processes interact to shape mountain landscape through a network of tightly coupled feedbacks⁹. It is being recognized that large-scale variations in structures and geomorphology near mountain front are the product of interaction between active dynamics and contemporary climate change.

As part of a palaeo-seismological study along the HFT, various geophysical methods (electromagnetic (EM) sounding, refraction seismic tests, high-resolution electrical resistivity tomography (HERT), ground-penetrating radar (GPR) and reflection seismics) can be used to locate and image an active fault zone at a depth range between a few decimetres and a few tens of metres. These geophysical studies along with geomorphological and geological data helped to locate trench excavations sites exposing the fault surfaces. The results were compared with the observations from the trench excavated from the

*For correspondence. (e-mail: akmahajan@rediffmail.com)

experimental site across the scarp. Similar effort has been done using two geophysical methods to test an already excavated site, where the presence of tectonic-controlled fault is demonstrated by trench log⁶ to know the efficacy and sensitivity of these methods in detecting faults.

Secondly, to track climate–tectonic-induced sub-surface changes like development of palaeo-channels or dissolution features, multichannel analysis of surface waves (MASW) has proved to be a promising method. The existence of these channels is examined along the exposed sections on the eroded stream banks. Both geophysical techniques allow images of near-surface features from a few metres to tens of metres, and offer faster and cost-effective solutions. In this article, we have applied MASW and HERT to test the resolution and sensitivity of these methods in imaging the near surface in terms of

shear wave velocity (V_s) and electrical resistivity distribution for detecting palaeo-channels. The experiment has been conducted on the bank of Tons River at Anarwala site, Uttarakhand, where the existence of such features had already been suggested by various researchers, while carrying out geomorphological, tectonic and climatic implications of Quaternary alluvial fan sedimentation^{10,11}.

Methodology

Two areas selected for geophysical imaging are located in proximity of the Himalayan mountain front, represented by the HFT (shown as rectangles in Figure 1a). The first site is located on the terrace deposits of the Gaggar river as it flows out of the mountain front near Chandigarh at Panchkulla, Haryana (Figure 1b). The other site is located on fan sediments of Doon valley at Anarwala.

Panchkulla site

This site is located on the campus of Government Degree College, Panchkulla, Haryana, which is about 9 km from Chandigarh on the Chandigarh–Dehradun highway (Figure 1b). The geologically documented trench⁶ was excavated east of the main entrance gate of the College. Geologically, the site is located on the terrace deposits of the Gaggar River¹⁰. The sediment succession of the Gaggar terrace comprises mainly of alluvial deposits made up of cobbles-boulder size sandstone clasts along with fine-grained fluvial and lacustrine deposits. Kumar *et al.*⁶ prepared the litholog of the area by excavating the 40 m long, 5 m wide and 7 m deep trench. Litho-section constructed by them has been re-drawn in Figure 2. The seven litho-strata identified by them have been marked as units 1–7. Unit 1 is composed of well-sorted clast-supported cobble gravels of fluvial origin; Unit 2 is dominated by matrix-supported pebbles–cobbles and gravels; Unit 3 consists of well-rounded, well-sorted pebble–cobble gravels of fluvial origin; Unit 4 has a thick material of extensively bio-turbated silty sand; Unit 5 shows alternating silt and fine-grained sand; Unit 6 has massive silty sand deposit with poorly sorted pebbles and cobbles, and unit 7 comprises alternating thin beds of fine-grained silt and sand (Figure 2).

Kumar *et al.*⁶ noted that gently dipping unit 3 bends abruptly at the crest of the topographic scarp causing displacement of litho units on either side (Figure 2). Unit 4 exposed on the northeast part of the profile is traced as a bottom layer across the bend providing evidence of a shallow fault with down throw of ~5 m. The displacement of different litho-units and presence of carbon helped them to identify the fault and give the possible date of occurrence of a historical earthquake.

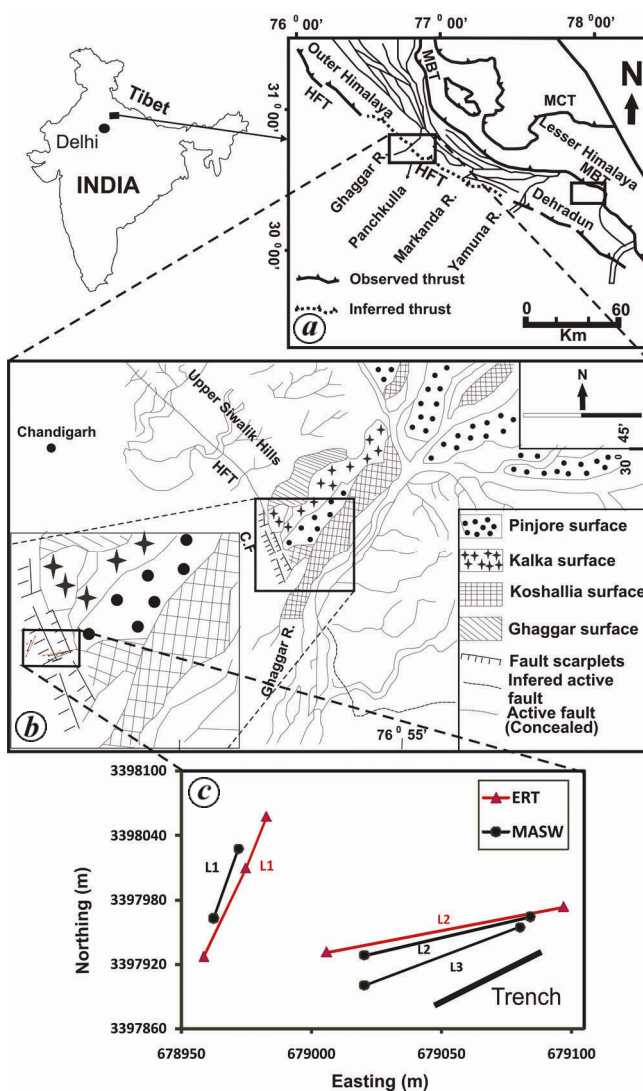


Figure 1. a, Geotectonic set up of Northwest Himalaya with location of study areas (rectangles). b, Location of active fault trace. c, Orientation of the multichannel analysis of surface waves (MASW) and high-resolution electrical resistivity tomography (HERT) profiles.

Anarwala site

This site is located in the northwestern part along the Tons river in an intermontane valley called ‘Doon’, within the Siwalik foreland basin of Garhwal Himalaya (Figure 3a). The location of the study area and its regional tectonic setting are shown in Figure 1a. The Doon valley is a crescent-shaped longitudinal synclinal valley controlled by a series of neotectonic faults traversing northeast-southwest and displacing the MBT^{1,12}.

The MBT separates Doon valley from the mountain scarp of the Mussoorie Ranges (Lesser Himalaya). Uplifted high-level fan terraces overstep the MBT, and the principal fans are deeply dissected at the foot of the mountain. The Doon valley is underlain by pebble and gravel deposits, which form the thick stratigraphic column of the valley and cover the major part of Dehradun city. Sites with shear wave velocity sections are shown as red circles in Figure 3. The sites are shown in the back-drop of geology and tectonic elements of Dehradun fan and adjoining fans.

According to the recent MASW survey, the probable thickness of Doon gravels was estimated to be 20–140 m. The cross-section of shear wave velocity profiles from north to south shows that high velocity material has been encountered at different sites, except the middle part of the fan where the bedrock is located at a depth of ~140 m (refs 13–15). Auden¹⁶ postulated that the Doon gravels are underlain by Upper Siwalik deposits. This does not differ much from the Doon gravels, except the northern part, where the Siwalik rocks can be seen on the surface that comprises mainly sandstone.

Landsat image map shows the location of Anarwala site, where the MASW and HERT profiles have been taken. To the northeast of the site (locally called football

ground), the Tons River flows from east to west (Figure 3b) and the deep dissected dry channel observed in the southwest–northeast direction, is well exposed on the northeast face of the football ground towards the river side. Field studies of the Anarwala site suggest that the topmost part of the exposed section comprises mainly boulders and pebbles mixed with yellowish-brown mud deposits. Beneath this compact and dissected Doon gravels consisting of small pebbles and gravel can be traced. Examination of the river cut-section on the northeastern face can be construed to indicate the presence of a number of channels draining the river from southwest to northeast direction. Figure 3c shows the direction of profiles obtained from the MASW and HERT techniques.

Analysis and processing

The physical principle, data acquisition and reduction steps of both methods, i.e. MASW and HERT are now well known, but for completeness and to illustrate their applicability for the present study, some basic aspects are briefly described below.

Multichannel analysis of surface waves

The MASW method belongs to the class of surface wave methods that uses the dispersive properties of fundamental mode Rayleigh waves to characterize the media in terms of shear wave velocity (for review see ref. 17). In early formulations, spectrum analysis of surface waves (SASW), ground roll generated by impulsive source and recorded by a pair of receivers were used to derive near-surface shear wave velocity profiles¹⁸. Given the sensitivity of shear wave velocity to stiffness, SASW has a number of applications in geotechnical engineering projects^{19,20}. Extending the concept to gather data in multichannel mode, formulation of MASW, including data acquisition using roll-along techniques, stacking multi-shot gather to enhance signal-to-noise ratio, extraction of dispersion curves and inversions to yield velocity–depth profiles were developed in a series of studies^{21–23}. The multichannel recordings from large receiver spread permit (i) identification of different types of seismic waves from their arrival and attenuation pattern²¹ and (ii) characterization of noise like direct waves, refracted waves, guided waves, air waves as well as higher modes of surface waves²⁴. These advantages coupled with the combination of roll-along acquisition format and use of generalized logarithmic inversion technique (GLT) have made MASW an effective and time-efficient method for imaging two-dimensional *S*-wave velocities for a variety of geological²², engineering and geo-hazard studies^{14,25–27}.

An 8 kg sledge hammer was used as the source and propagating surface wave was recorded using 24-channel

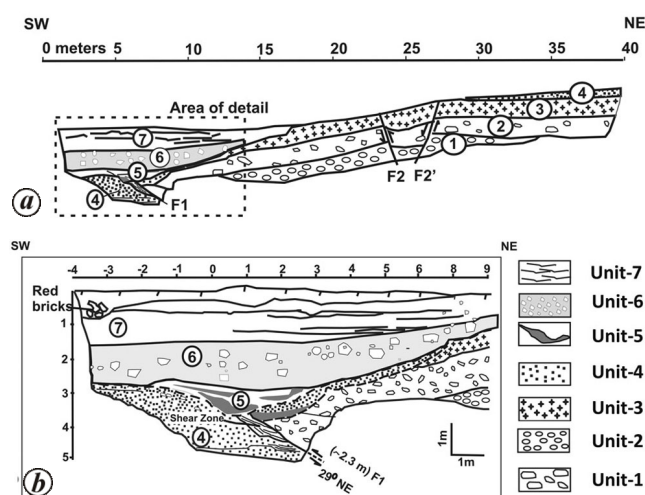


Figure 2. a, Litholog of the trench excavated at Panchkulla; b, Enlarged section of dotted rectangle in (a), where fault has been demarcated by the ~5 m displacement of litho unit 4 (ref. 6).

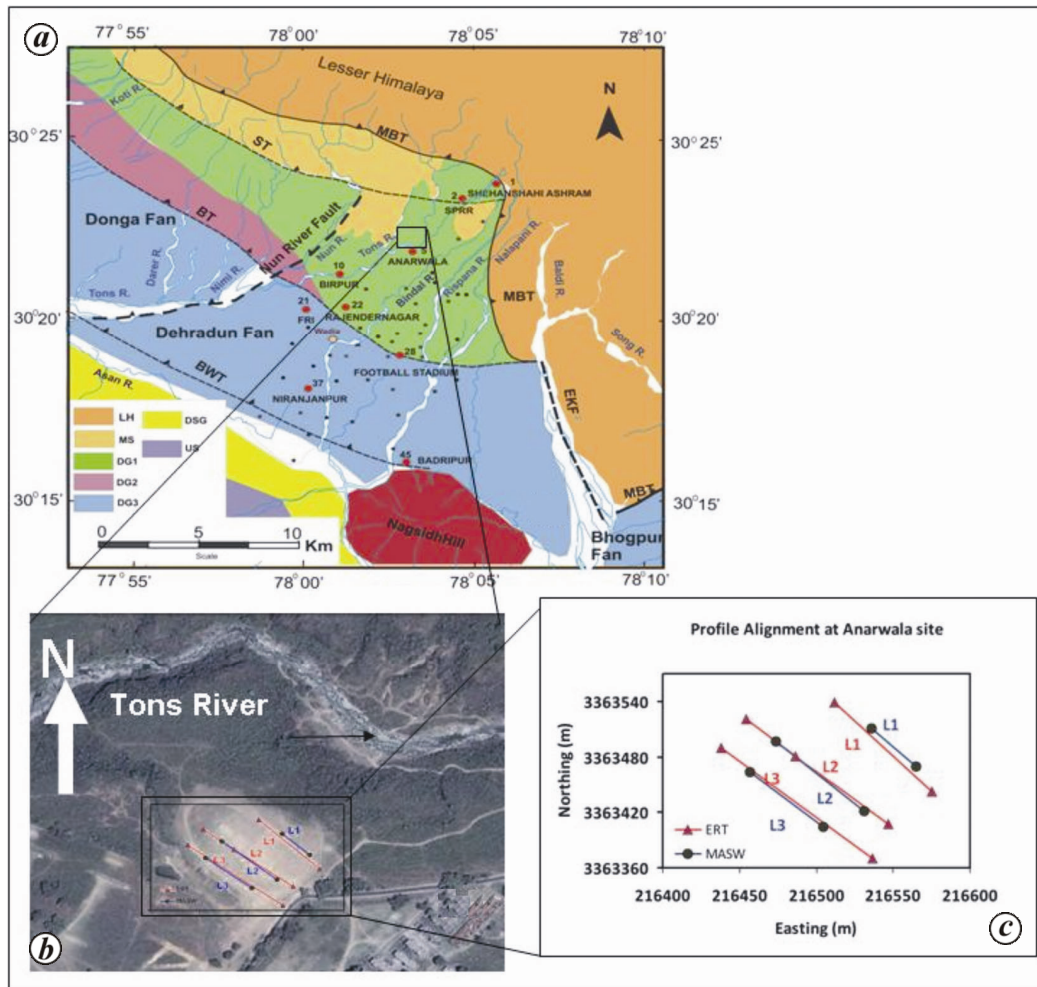


Figure 3. *a*, Regional geo-tectonic map with location of study area (rectangle). *b*, Morphological feature around the study area. *c*, Orientation of different geophysical profiles. MFT, Main Frontal Thrust; BT, Bhauwala Thrust; BWT, Bansiwala Thrust; NRF, Nun River Fault; EKF, East Kalinga Fault; LH, Lesser Himalaya; US, Upper Siwalik; MS, Middle Siwalik. The classification of Dehradun fan gravels is from ref. 12; DG-1, Doon gravel units A–C; DG-2, Doon gravel units B and C; DG-3: Doon gravel unit C; DSG, Dip slope gravels. (Inset) Location of three Duns in NW Himalaya (top) and regional tectonic map of Doon valley (bottom).

Geometrics Geode unit with 14 Hz geophones, each placed 2 m apart. Multiple numbers of shot gathers were collected along a linear survey line of 72–96 m by moving both the source and the receiver spread in a manner similar to common depth point (CDP) roll-along technique used in conventional seismic reflection survey. To achieve long profile length, three different settings of the source with respect to the geophone spread were used. In the near, middle and far positions, the first shot point was located at 2, 26 and 50 m respectively, from the first geophone of the spread. For each geometrical configuration set-up, the deduced velocity profile is a representative of the material directly beneath the middle of a geophone spread.

The raw field data possess strong ground roll of surface waves, which are enhanced by stacking the multi-shot gathers for each geophone. The entire data processing was carried out using SurfSeis 1.5 and 2 software²⁸,

developed by the Kansas Geological Survey, Kansas, USA. It was found that the extracted frequency range and phase velocities were significantly different at the two sites, due to difference in the compaction of sediments. The penetration depth of ground roll was approximately equal to its wavelength (λ)²⁹, whereas shear wave velocities could be reasonably calculated to a depth (Z_{\max}) about half the longest wavelength (λ_{\max}) measured³⁰. It has been shown that surface waves at higher frequencies attenuate rapidly with distance, away from the source. It has also been suggested that the lowest extracted frequency (f_{\min}) determines the maximum depth of investigation Z_{\max} such that

$$Z_{\max} = C/(2f_{\min}), \quad (1)$$

where C is the phase velocity at frequency f_{\min} . Substituting values from Figures 4 *a*, *b* and 5 *a*, *b*, Z_{\max} probed at

Panchkulla and Anarwala sites was found to be of the order of 18–20 m and 50–55 m respectively. It is clear that despite similar field configurations, the depth investigated varied significantly largely due to the intrinsic material properties at the respective sites, particularly stiffness. Inversion of dispersion curve at each geophone point, using the algorithm developed by Xia *et al.*²³, provided 1D shear wave velocity profile. Since the inverted model provided a satisfactory fit to the observed features of the dispersion curve, the 1D approximation for velocity–depth profiles was validated, using field observations and bore hole data^{13–15}. Therefore, gathering all 1D velocity profiles into shot station sequential order was interpolated as continuous 2D shear wave velocity cross-section along the survey line.

As an illustration of the processing part, the raw multi-shot data gathered with their dispersion curve and 1D velocity profiles are shown in Figures 4 and 5 respectively, for Panchkulla and Anarwala sites. Figure 4 shows the Panchkulla site seismic record nos 113 and 123 and their dispersion curves and inverted 1D profile. Similarly, Figure 5 shows the Anarwala site record nos 102 and 118 with their dispersion curves and corresponding inverted 1D velocity models. However, to strengthen the accuracy, in the derived dispersion curves and their inverted velocity profiles, two dispersion curves and their corresponding inverted 1D profiles have been shown in each figure. At Anarwala site, the change in velocity with depth in two consecutive mid-station locations, reflects the change in stiffness of the material within and outside the channel, whereas above the channel the velocity values are almost the same.

High-resolution electrical resistivity tomography

Among all geophysical methods, electrical resistivity prospecting, is the most commonly applied for near-surface imaging. Electrical resistivity by virtue of its sensitivity to lithology, intrinsic properties, porosity, fractures, degree and nature of fluids filling the pores, etc. makes resistivity images an ideal tool for hydrological studies as well as for mapping near-surface features related to tectonic deformation, chemical solution activities and changes that occur due to the variation in saturation level, etc. The direct-current four electrodes configuration is widely used for the acquisition of field data, allowing estimation of resistivity–depth profiles. However, the extent to which estimated resistivity–depth profiles are affected by horizontal changes in the subsurface resistivity remains largely unresolved. This limitation is greatly circumvented, using more advanced and powerful formulation of HERT employing multi-electrode system³¹. The multi-electrode system facilitates imaging lateral variations more precisely, due to dense measurements with overlapping spacing^{31,32} and hence HERT becomes more appli-

cable to heterogeneous regions^{33,34}. The number of data points produced by such high-resolution surveys is more than twice that obtained with a conventional array and hence a better area coverage and resolution can be achieved. Because of its high resolution and greater sensitivity in delineating the lateral heterogeneity, it has been applied in the Himalayan foothills, to decipher the near-surface features related to tectonic and chemical solution activities.

A Syscal Pro-72 system equipped to use maximum of 72 electrodes with provision of inter-electrode separation up to 10 m has been used for the present survey. A 2 m inter-electrode separation with Wenner–Schlumberger configuration was used for one-to-one comparison with MASW results and for obtaining high resolution at shallow depth range. The median depth of investigation in HERT for Wenner–Schlumberger arrays is roughly 0.191 m of the maximum electrode separation³⁵. With a total of 72 electrodes and maximum 32 levels of measurement, the experiment is designed to yield investigation depth of around 23 m. The RES2DINV program (obtained from the supplier of the equipment, M/s IRIS instrument, France; <http://www.iris-instruments.com/>) was used for

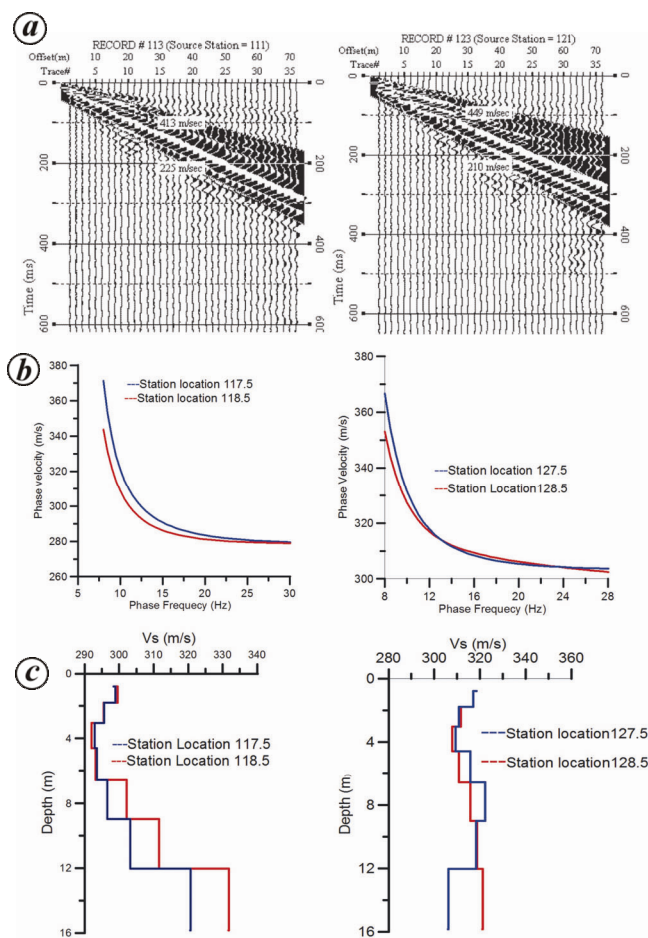


Figure 4. *a*, Raw seismic data with multi shot surface wave roll; *b*, Extracted dispersion curve; *c*, Inverted 1D velocity–depth profile for different records of Panchkulla site.

inversion. This utilizes an iterative method where starting from an initial model, the program tries to find an improved model, whose calculated apparent resistivity values are closer to the measured values³³.

Field operation

At the Panchkulla site, both MASW and HERT surveys were conducted along three lines (L1, L2 and L3) shown in Figure 1 *b, c*. Under the surface cover of overbank deposits, a fault with overall vertical displacement of about 5 m is indicated in the excavated trench section⁶. Civil construction inhibited spreading of survey lines across the identified fault line in the trench. Lines L2 and L3, placed about 25 m of the trench run across the topographic scarp, which appears to define the surface track of the fault mapped in the trench. Line L1 is oblique to the strike of suspected fault zone. Thus, a joint study of MASW and HERT was carried out along these three lines to identify and confirm the nature and depth extent of a geologically documented fault.

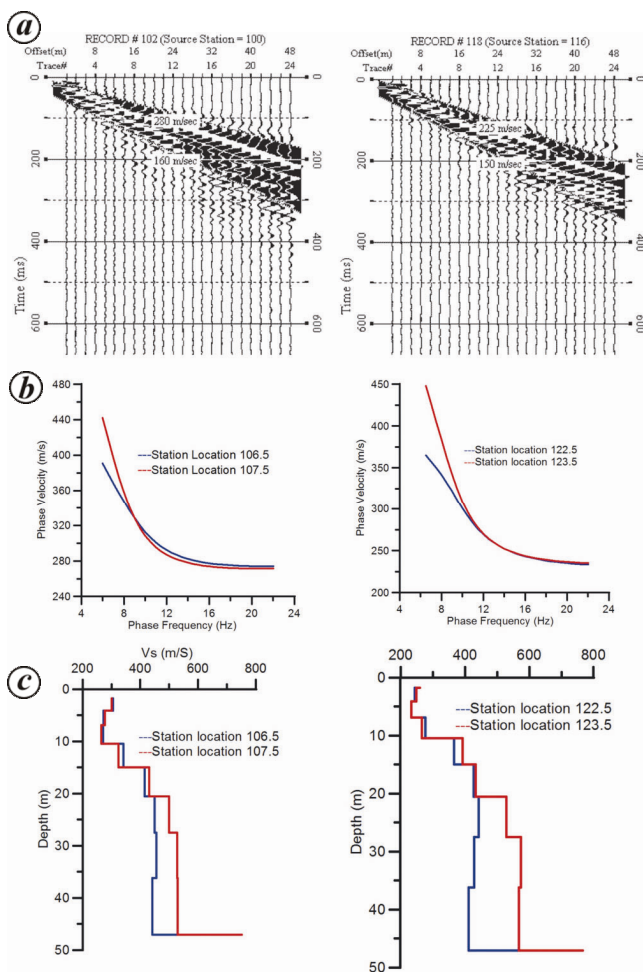


Figure 5. *a*, Raw seismic data with multi shot surface wave roll; *b*, Extracted dispersion curve; *c*, Inverted 1D velocity–depth profile for different records of Anarwala site.

The Anarwala site was surveyed earlier as part of the microzonation study of Dehradun city¹⁴. A single MASW survey conducted along a line in the Anarwala ground south of the Tons River. The inverted velocity cross-section indicated deep-cut cavity structures, marked as low-velocity enclosures. In order to constrain further the geometry, direction and extent of suggested presence of palaeo-channel and/or erosional features at the Anarwala site, three closely spaced parallel profiles on the terrace ground were identified for joint MASW and HERT surveys (Figure 3 *b* and *c*). To the north of the survey ground, the Tons River flows east to west, and deep vertical river cut allows full view of the stratigraphy and exhibits deep channels. To the southwest of the study area, a wide, low-lying depression forms the primary topographic feature, while south and east of the Anarwala site display flat topography. All three transects are aligned in NW–SE direction to excite maximum response from NE–SW directed structures (Figure 3 *c*).

The data for all transects were identically processed using the respective approaches described in earlier sections. The important structural inferences became possible due to concurrent application of different geophysical approaches. The deduced 2D sections of velocity and resistivity distribution have been used for tectonic and structural interpretation in the following sections.

Results and discussion

Geophysical identification of near-surface fault at Panchkulla

The processing of MASW and HERT profiles at Panchkulla produced nearly identical results. Figure 6 *a, b* shows the typical inverted velocity and resistivity cross-section along line L2. The most conspicuous feature of shear wave velocity (V_s) cross-section along line L2 (Figure 6 *a*) is the sharp transition in V_s in the upper surface layer of ~6 m thickness. It is noted that sediments on the southwest part of the profile from geophone locations 105 to 121 are marked by moderate velocities of the order of 250 m/s. Across the geophone locations 122 and 123, V_s jumps over to about 350 m/s. High V_s (350 m/s) corresponds to litho unit 3 (Figure 2) that is exposed at the northeast part of the site and comprises light brown, well-sorted pebbles–cobbles, fluvial thick layer gravels with sand and pebble-supported matrix. The velocity transition coinciding with topographic scarp is completely in agreement with the trench section, where nearly flat litho unit 3 bends abruptly at the crest to define the fault zone⁶. The litho unit 4 exposed on the hanging wall and tracked in the bottom part of the trench section allows estimation of the vertical down throw of approximately 5 m along the fault (Figure 2). The evidence that surface high-velocity layer mapped on the NE part of line L2 continues

southwest, though somewhat discontinuously, under the cover of moderate velocity layer, provides confirmation to the steeply dipping fault with overall vertical displacement of 5–6 m (Figure 6a). The extended cross-section also warrants, that displaced strata continue beyond both ends of the excavated trench.

The scattering of hammer-generated surface waves by recent near-surface river deposits (gravel and pebble-rich layer) restricts the depth penetration; therefore, MASW imaged velocity distribution was limited to a depth of 10–15 m. By contrast, the HERT experiment provided resistivity images roughly to a depth of 23 m. The 2D resistivity–depth section beneath line L2 (Figure 6b) as well as along line L3 indicates a two-layered structure. The top layer extending roughly up to a depth 8 m has relatively high resistivity, varying in range between 120 and 300 Ωm (Figure 6b). The bottom layer is characterized by relatively low resistivity of the order of 20–80 Ωm. In addition to a possible lithological transition, the low resistivity of the second layer may be caused by variation in

the degree of saturation in the subsurface succession. Such visualization is supported by the depth to water table that is around 10 m in a number of tube wells in the region. More striking is that in contrast to the marked lateral variation in velocity (Figure 6a), the top layer along the total length of the profile is characterized by near-uniform high resistivity, except that the resistivity section unambiguously depicts a break, to define tilted, low-resistivity anomaly coinciding with the fault zone, in the trench section (Figure 6b).

Computations were carried out using the algorithm RES2DMOD³⁵. The aim of this forward modelling was not to simulate the features of the inverted resistivity section in totality, but only to test whether such fault models can reproduce breaks in resistivity. The trial and error runs of the synthetic model showed that most salient features of the breaks in the upper resistivity section could be reproduced (Figure 6c) when the inclined (~45°) fault plane with limited width is simulated by low resistivity (30 Ωm) and extends in depth no more than 8–10 m. Constraining the dip and magnitude of displacement across the fault by the trench section, it was found that resistivity contrast arising from displacement of different strata across the fault, could not reproduce signatures of the observed break in resistivity section (Figure 6d). Since resistivity of the inclined plane is lower than the individual layers at different depth sections, the fault trace can be interpreted as a moisture-rich zone. In order to constrain the presence of fault seen within the trench, in MASW profile and in also resistivity profile, electrical resistivity tomography (ERT) response was computed for the synthetic Panchkulla fault model (Figure 6e). In the synthetic resistivity model, the different layers with marginal offset across the fault (Figure 6e) were assigned resistivities to simulate resistivity–depth distribution as observed in the inverted resistivity section (Figure 6b). In the synthetic model, the fault-associated displacements are considered to extend beyond the depth excavated in the trench because resistivity break coinciding with fault location in the upper 8 m section is seen to extend into deeper sections up to ~20 m (Figure 6e).

Applications of MASW and HERT across the geologically documented fault in sedimentary environment have shown contrasting response. Despite the noted transition in lithology across the fault in trench section (Figure 2), the laterally uniform resistivity distribution on line L2 (Figure 6b) warrants that sedimentary sequences on either side of the inferred fault are not marked by sharp contrast in physical properties. In case of the deduced resistivity section, the fault plane marked by break in resistivity (Figure 6b) could be associated with the increased state of saturation (Figure 6e). Given these evidences, the observed sharp velocity change at this location (Figure 6a) may characterize sharp change in the degree of stiffness or rigidity of the medium in the upper 6 m thick section. The sensitivity of shear wave velocity to degree of

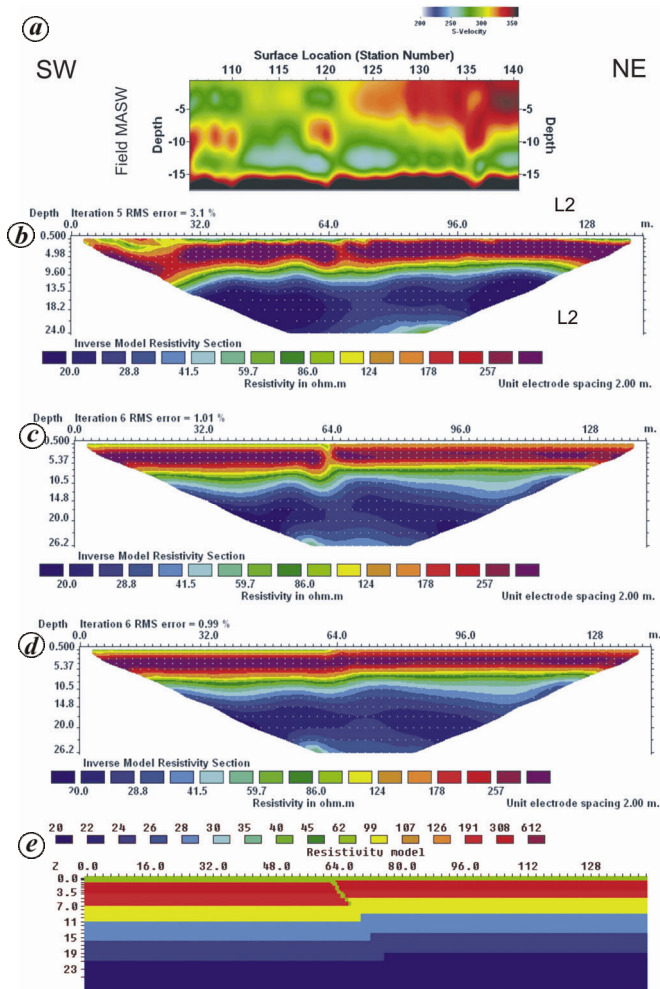


Figure 6. a, Shear wave velocity; b, deduced resistivity profile; c, simulated HERT response; d, without simulating the top 7 m; e, derived synthetic resistivity model of Panchkulla site.

stiffness was the key motivation for adoption of MASW for engineering purposes³⁶.

Geophysical signatures of erosional features/ palaeo-channel at Anarwala

The MASW survey along three lines at Anarwala permitted to extract dispersion curves invariably for a band from 8 to 20 Hz. The inversion of these curves allowed estimation of shear wave velocity to a depth section up to 45 m. The stitched 2D velocity–depth profiles for three NW–SE trending lines L1, L2 and L3 show near-identical velocity sections (Figure 7). The velocity sections to the full depth of investigation typically show four-layered structure. The top layer (6–10 m thick) has a shear wave velocity of 250–300 m/s, whereas the second layer located in the depth range 6–22 m has velocities peaking to ~450 m/s. The low velocities in the upper layer correspond to a pile of sediments comprising gravel of different sizes ranging from 2 to 4 mm embedded in silty matrix of the Lesser Himalayan source. Marginal velocity increase in the lower part is ascribed to the presence of alternating compact silty mud and sand. The substratum at depth, marked by extremely high velocity of >750 m/s, can be viewed as bedrock to the fan deposits.

The velocity contours in the middle depth section, roughly between 20 and 40 m, display multiple low-velocity zones embedded in high-velocity enclosures.

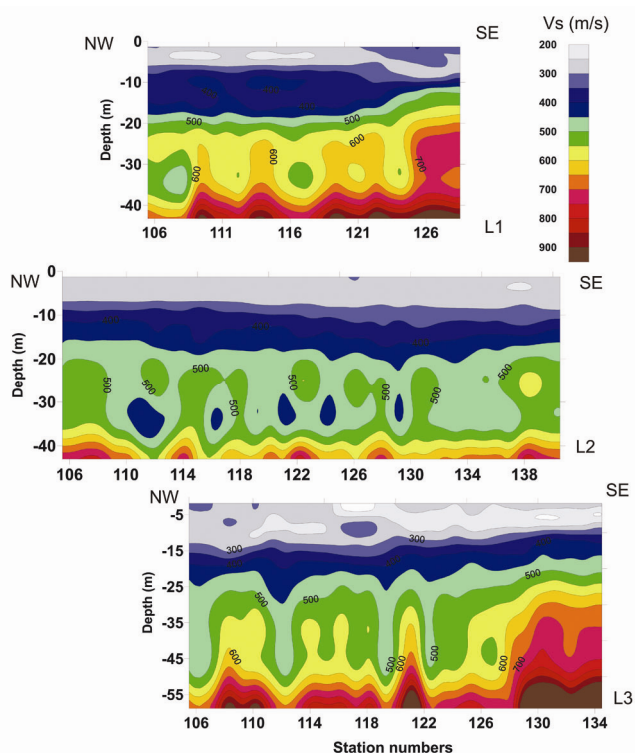


Figure 7. Shear wave velocity cross-section along three lines – L1 (northern), L2 (central) and L3 (southern) at Anarwala site.

Given that high rate of sedimentation and climate-driven erosion/weathering were rampant during the evolution of the Doon valley¹¹, low-velocity zones can be viewed as erosional channels etched into already deposited sediments (stiff in strength)/bedrock surface. It was noted that the presence of low-velocity enclosures is characterized by the presence of dissected Doon gravels, as also reported by Nakata¹⁰. According to Singh *et al.*¹¹, during the initial phase of evolution of the Doon fan, fluvial gravels were deposited by high-energy streams emerging from hinterland. Subsequently, these gravel beds were dissected by the erosion of old sediments and the eroded portion was filled with fresh deposits. The material filling the eroded portion was drawn from the erosion of the same host rocks; so there may not be strong lithological contrast. Despite the fact that shear wave velocity cannot be an analogy of any lithology, the channel-like structures are well observed because shear wave velocity is sensitive to the compaction of material. The presence of channel structures is in agreement with field investigations, as one can see channel openings on the headward side of the wall of the ground along the Tons River valley. The velocity images produced as a result of the present study clearly indicate the geometry and depth extent of three palaeo-channels. The three channels that pass under the ground from SW to NE direction are mapped below geophone locations 112, 117 and 124 on the northern line L1; 112, 116 and 134 on the central line L2, and under geophones 112 and 119 on the southern line L3 (Figure 7). The curvilinear features, identified as palaeo-channels, were seen below station locations 112, 124 on line L1; 112, 116, 129 on line L2, and 112, 120 on line L3.

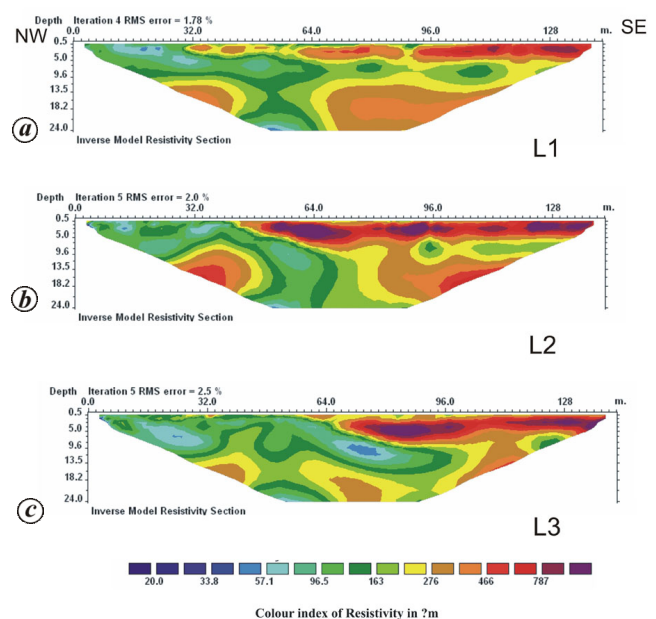


Figure 8. Inverted resistivity cross-section along three lines – L1 (northern), L2 (central) and L3 (southern) at Anarwala site.

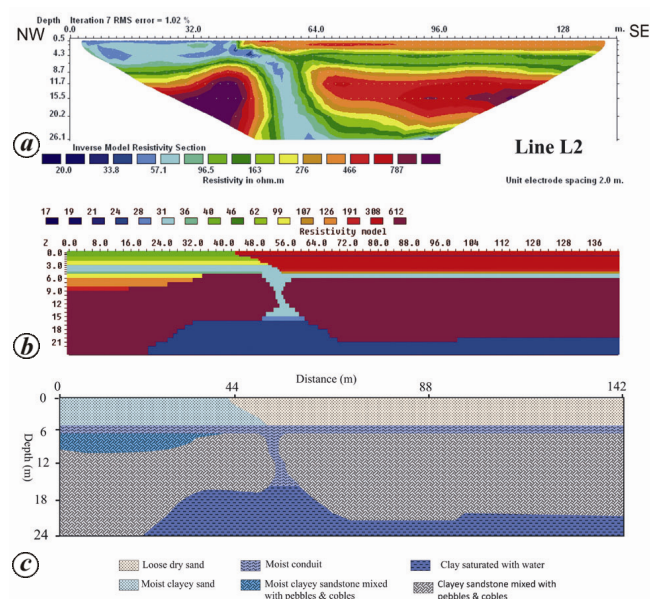


Figure 9. *a*, Deduced HERT resistivity profiles; *b*, Computed synthetic model; *c*, Conceptualized hydrological model along line L2 at Anarwala site.

The 2D resistivity sections obtained by the inversion of HERT data along the same three parallel lines provide resistivity images only for the upper 25 m (Figure 8) and thus inhibit validation of palaeo-channel-like features noted on MASW survey derived from shear wave velocity structure. However, the inverted resistivity distribution brings out certain anomalous features (may be palaeo-channel), which apparently reflect the hydrological drainage of the fan. On line L3, there is a suggestion of inclined extended low-resistivity zone on the northwest part of the profile. The low-resistivity zone ($\sim 40\text{--}50\ \Omega\text{m}$) extends from near surface to a depth of 12 m in the central part of the profile. Below lines L1 and L2, the steep-dipping low-resistivity feature in the central part of the profile is seen to extend as a sub-vertical structure. The synthetic 2D resistivity model (Figure 9*b*) shows that HERT response (Figure 9*a*) reproduces the observed features on lines L1 and L2 (Figure 8*a* and *b*), which equally help to view this dipping low-resistivity zone as a narrow vertical structure from a shallow depth of 6 to 18 m (Figure 9*b*). The surveyed fan terrace on the southwest is flanked by an extended depression of 2–3 m depth. The depression serves as a watershed during the monsoon period. A hydrological model is conceptualized (Figure 9*c*), wherein the flat, low-resistivity layer mapped at a depth of 3–4 m on the northwest part of profile (Figure 9*a–c*) serves as a hydrological drain for groundwater to flow out from the depressed area. The flow of water through the drain provides a link to the vertical channel-like structure that serves as duct to divert the water flow to the valley. The increased saturation of such vertical channel facilitates it to be mapped as low-resistivity enclosure.

Conclusions

This article discussed the results of a pilot experiment undertaken to test the efficacy and sensitivity of MASW and HERT techniques individually to investigate near-surface features in sedimentary environment of mountain front of the Northwest Himalaya. Due to the absence of sharp contrast in physical properties amongst various sedimentary sequences, the imaged shear wave velocity or resistivity distribution has poor resolution in providing litho-compatible stratification. However, by virtue of their sensitivities to stiffness, degree of saturation, etc. the deduced velocity and/or resistivity sections are effective in locating and mapping structural features, including near-vertical displacement. The latter is in agreement with the geologically recognized fault, in the terrace deposits on the bank of Gaggar River. The MASW technique has shown great promise in detecting voids, palaeo-channels and erosional features that are characteristic of the tectonic-evolutionary history of the Dehradun fan. The resistivity distribution, when combined with the synthetic modelling, further helps to construct the geometry and extent of the involved structures. Given the sensitivity of resistivity to the degree of saturation, an integration of resistivity signatures with hydrology could be used to trace the role of near-surface channels in draining and the water cycle of the region. In the sedimentary dominant environment of the frontal Himalaya, the velocity and/or resistivity sections deduced from the application of the MASW and the HERT techniques, have proved effective in locating and mapping the fault zone or subsurface, e.g. palaeo-channels that are characteristic of the tectonic-evolutionary history of the study region. The suggestion of a steeply dipping fault, with an overall vertical displacement of 5 m near Panchkulla, inferred from the observationally reduced velocity section, is in agreement with the fault recognized in the trench. Given the sensitivity of resistivity to the degree of saturation, an integration of resistivity with hydrology could be used to trace the role of near-surface channels in draining the water of the region. Both sites have been studied for site characterization due to their location in earthquake-prone region.

1. Thakur, V. C., *Geology of the Western Himalaya*, Pergamon Press, London, 1992, p. 362.
2. Seeber, L. and Armbruster, J., Great detachment earthquakes along the Himalayan Arc and long-term forecasting. In *Earthquake Prediction – International Review* (eds Simpson, D. W. and Richards, P. G.), American Geophysical Union, Washington, DC, 1981, pp. 259–277.
3. Ni, J. and Barazangi, M., Seismotectonics of the Himalayan collision zone: geometry of the under thrusting Indian plate beneath the Himalaya. *J. Geophys. Res.*, 1984, **89**, 1147–1163.
4. Kayal, J. R., Micro earthquake activity in some parts of the Himalaya and the tectonic model. *Tectonophysics*, 2001, **339**, 331–351.
5. Gahalaut, V. K., Major and great earthquakes and seismic gaps in the Himalayan arc. *Mem. Geol. Soc. India*, 2008, **66**, 373–393.
6. Kumar, S., Wesnousky, S. G., Rockwell, T. K., Briggs, R. W. and Thakur, V. C. and Jayangondaperumal, R., Paleoseismic evidence

- of great surface-rupture earthquakes along the Indian Himalaya. *J. Geophys. Res.*, 2006, **111**(B3), B03304; doi: 10.1029/2004JB003309.
7. Javed, N. M. and Nakata, T., Active faults and related late Quaternary deformation along the north-western Himalayan Frontal zone, India. *Ann. Geophys.*, 2003, **46**(5), 917–936.
 8. Lave, J., Yule, D., Sapkota, S., Basant, K., Madden, C., Attal, M. and Pandey, R., Evidence for a great medieval earthquake (~1100 AD) in the Central Himalayas, Nepal. *Science*, 2005, **307**, 1302–1305.
 9. Sinha, S., Sangode, S. J., Kumar, R. and Ghosh, S. K., Accumulation history and tectonic significance of the Neogene continental deposits in the west central sector of the Himalayan foreland basin. *Himalayan Geol.*, 2005, **26**, 387–408.
 10. Nakata, T., Active faults of the Himalaya of India and Nepal. *J. Geol. Soc. Am. Spl. Paper*, 1989, **232**, 243–264.
 11. Singh, A. K., Prakash, B., Mohindra, R., Thomas, J. V. and Singvi, A. K., Quaternary alluvial fan sedimentation in the Dehradun valley, Piggyback basin, NW Himalaya: tectonic and palaeoclimatic implications. *Basin Res.*, 2001, **13**, 449–471.
 12. Thakur, V. C. and Pandey, A. K., Late quaternary tectonics evolution of Dun in fault bend/propagated fold system, Garhwal sub-Himalaya. *Curr. Sci.*, 2004, **87**(11), 1567–1576.
 13. Mahajan, A. K. and Nitesh, R., Using MASW to map depth to bedrock underneath Dehradun Fan deposits in NW Himalaya. *Curr. Sci.*, 2011, **100**(2), 233–238.
 14. Mahajan, A. K., Sporry, R. J., Champati, P. K., Rajiv, R., Slob, S. and Westen, C. V., Seismic micro zonation of Dehradun city using geophysical and geotechnical characteristics in the upper 30-meters of soil column. *J. Seismol.*, 2007, **11**, 335–370.
 15. Mahajan, A. K., NEHRP soil classification and estimation of 1-D site effect of Dehradun fan deposits using shear wave velocity. *Eng. Geol.*, 2009, **104**, 232–240.
 16. Auden, J. B., The structures of the Himalaya in Garhwal. *Rec. Geol. Surv. India*, 1936, **71**, 409–433.
 17. Steeples, D. W. and Miller, R. D., Basic principles and concepts of practical shallow seismic reflection profiling. *Min. Eng.*, 1993, **45**, 1297–1302.
 18. Nazarian, S., Stokoe, K. H. and Hudson, W. R., Use of spectral analysis of surface wave method for determination of moduli and thickness of pavement. *Transp. Res. Rec.*, 1983, **930**, 38–45.
 19. Gucunski, N. and Woods, R. D., Instrumentation for SASW testing. In *Recent Advances in Instrumentation, Data Acquisition and Testing in Soil Dynamics* (eds Bhatia, S. K. and Bilaney, G. W.), American Society of Civil Engineering, 1991, pp. 1–16.
 20. Stokoe II, K. H., Wright, G. W., James, A. B. and Jose, M. R., Characterization of geotechnical sites by SASW methods. In *Geophysical Characterization of Sites* (ed Wood, R. D.), Oxford Publication, 1994.
 21. Park, C. B., Miller, R. D. and Xia, J., Imaging dispersion curves of surface waves on multichannel records. Technical programme with biographies. In SEG, 68th Annual Meeting, New Orleans, Louisiana, 1998.
 22. Miller, R. D., Xia, J., Park, C. B. and Ivanov, J. M., Multichannel analysis of surface waves to map bedrock. *Leading Edge*, 1999, **18**, 1392–1396.
 23. Xia, J., Miller, R. D. and Park, C. B., Estimation of near surface shear wave velocity by inversion of Rayleigh waves. *Geophysics*, 1999, **64**, 691–700.
 24. Ivanov, J., Park, C. B., Miller, R. D. and Xia, J., Mapping Poisson's ratio of unconsolidated materials from a joint analysis of surface-wave and refraction events. In *Proceedings of the Symposium on the Applications of Geophysics to Engineering and Environmental Problems*, Arlington, Va., 20–24 February 2000.
 25. Street, R., Wooley, E. W., Wang, Z. and Harris, J. B., NEHRP soil classification for estimating site dependent seismic coefficients in the upper Mississippi Embayment. *Eng. Geol.*, 2001, **62**, 123–135.
 26. Mahajan, A. K., Galiana-Merino, J. J., Lindholm, C., Arora, B. R., Mundepi, A. K., Rai, N. and Chauhan, N., Characterization of the sedimentary cover at the Himalayan foothills using active and passive seismic techniques. *J. Appl. Geophys.*, 2011, **73**, 196–206.
 27. Mahajan, A. K., Mundepi, A. K., Chauhan, N., Jasrotia, A. S., Rai, N. and Gachhayat, T. K., Active seismic and passive microtremor HVSR for assessing site effects in Jammu city, NW Himalaya, India – a case study. *J. Appl. Geophys.*, 2012, **77**, 51–62.
 28. Park, C. B. and Brohammer, M., SurfSeis 1.5V software for multichannel analysis of surface waves, Kansas Geological Survey, Kansas, USA, 2003.
 29. Richart, F. E., Hall, J. R. and Woods, R. D., *Vibrations of Soils and Foundations*, Prentice-Hall, Inc, 1970.
 30. Rix, G. J. and Leipski, A. E., Accuracy and resolution of surface wave inversion. In *Recent Advances in Instrumentation, Data Acquisition and Testing in Soil Dynamics* (eds Bhatia, S. K. and Blaney, G. W.), American Society of Civil Engineering, Geotechnical Special Publication no. 28, 1991, pp. 17–23.
 31. Griffiths, D. H. and Barker, R. D., Two-dimensional resistivity imaging and modeling in areas of complex geology. *J. Appl. Geophys.*, 1993, **29**, 211–226.
 32. Loke, M. H., Electrical imaging surveys for environmental and engineering studies, A practical guide to 2-D and 3-D surveys, 2000, p. 67; <http://www.terraip.co.jp/lokenote.pdf>
 33. Chandra, S., Rao, V. A., Krishnamurthy, N. S., Dutta, S. and Shakeel, A., Integrated studies for characterization of lineaments to locate groundwater potential zones in hard rock region of Karnataka, India. *Hydrogeol. J.*, 2006, **14**, 767–777.
 34. Chandra, S., Dewandel, B., Dutta, S. and Ahmed, S., Geophysical model of geological discontinuities in a granitic aquifer: analyzing small scale variability of electrical resistivity for groundwater occurrences. *J. Appl. Geophys.*, 2010, **71**, 137–148.
 35. Edwards, L. S., A modified pseudosection of resistivity and induced-polarization. *Geophysics*, 1977, **42**, 1020–1036.
 36. Ansal, A., *Recent Advances in Earthquake Geotechnical Engineering and Microzonation*, Kluwer, 2004, p. 354.
- ACKNOWLEDGEMENTS. This paper is an outcome of a MoU signed between Wadia Institute of Himalayan Geology (WIHG), Dehradun and CSIR-National Geophysical Research Institute (NGRI), Hyderabad for joint studies in the field of subsurface investigations. We thank Dr V. P. Dimri (former Director, NGRI), Dr Shakeel Ahmed, Dr V. C. Thakur, Dr N. S. Virdi, Dr S. K. Ghosh and Dr Jayangondaperrumal for their useful suggestions; Dr Dewashish Kumar, Mr Sushobhan Dutta and Mr Kaushlendra Mangal Bhatt (NGRI) for help with data acquisition in the field; the Vice-Chancellor, Central University of Himachal Pradesh, Dharmashala for providing the necessary facilities. Thanks are also due to the Director, Wadia Institute of Himalayan Geology, Dehra Dun and Director, NGRI for providing research facilities and encouragement for undertaking this work.

Received 3 September 2014; revised accepted 18 March 2015